Aerosol Science and Engineering (2021) 5:499–515
https://doi.org/10.1007/s41810-021-00117-2

ORIGINAL PAPER

Overview and Seasonality of PM_{10} and $PM_{2.5}$ in Guayaquil, Ecuador

Daniel Moran-Zuloaga[1,2] · Wilson Merchan-Merchan[3] · Emilio Rodríguez-Caballero[4,5] · Philip Hernick[6] · Julio Cáceres[2] · Mauricio H. Cornejo[2]

Received: 6 March 2021 / Revised: 15 July 2021 / Accepted: 4 August 2021 / Published online: 17 August 2021

Abstract

The focus of this study is the assessment of total suspended particles (TSP) and particulate matter (PM) with various aerodynamic diameters in ambient air in Guayaquil, a city in Ecuador that features a tropical climate. The urban annual mean concentrations of TSP (Total Suspended Particles), and particle matter (PM) with various aerodynamic diameters such as: PM_{10}, $PM_{2.5}$ and PM_1 are 31 ± 14 μg m^{-3}, 21 ± 9 μg m^{-3}, 7 ± 2 μg m^{-3} and 1 ± 1 μg m^{-3}, respectively. Air mass studies reveal that the city receives a clean Southern Ocean breeze. Backward trajectory analysis show differences between wet and dry seasons. During the dry season, most winds come from the south and southwest, while air masses from the peri urban may contribute as pollutant sources during the wet season. Although mean values of PM_{10} and $PM_{2.5}$ were below dangerous levels, our year-round continuous monitoring study reveals that maximum values often surpassed those permissible limits allowed by the Ecuadorian norms. A cluster analysis shows four main paths in which west and southwest clusters account for more than 93% of the pollution. Total vertical column of NO_2 shows the pollution footprint is strongest during the dry season, as opposed to the wet season. A microscopic morphological characterization of ambient particles within the city during the wet and the dry season reveals coarse mode particles with irregular and rounded shapes. Particle analysis reveals that samples are composed of urban dust, anthropogenic and organic debris during the dry season while mainly urban dust during the wet season.

Keywords Coarse mode particles · Guayaquil · HYSPLIT · Seasonality · SEM–EDS analysis

Abbreviations

AOD_{550nm}	Aerosol optical depth 550 nm
CIDNA	Centro de Investigación y Desarrollo en Nanotecnología
ESPOL	Escuela Superior Politécnica del Litoral
GIOVANNI	Geospatial interactive online visualization and analyze infrastructure
HR SEM	High resolution scanning electronic microscopy image
HYSPLIT	Hybrid single particle Lagrangian integrated trajectory model
IC engines	Internal combustion engines
INOCAR	Instituto Nacional Oceanográfico de la Armada
LabFREE	Laboratory of free resources energy
LATAM	Latin American Airlines Group
MAE	Ministerio del Ambiente, Ecuador
NO_2	Nitrogen dioxide
PM_1	Particulate matter with aerodynamic diameter < 1 μm
PM_{10}	Particulate matter with aerodynamic diameter < 10 μm
$PM_{2.5}$	Particulate matter with aerodynamic diameter < 2.5 μm
TOPAS	Turnkey optical particle analysis system

✉ Daniel Moran-Zuloaga
dmoran@espol.edu.ec

[1] Department of Chemistry, Pharmacy and Geoscience, Johannes Gutenberg University Mainz, Saarstrasse 21, 55122 Mainz, Germany

[2] Centro de Investigación y Desarrollo en Nanotecnología (CIDNA), Escuela Superior Politécnica del Litoral (ESPOL), Guayaquil, Ecuador

[3] School of Aerospace and Mechanical Engineering, University of Oklahoma, Norman, OK 73019, USA

[4] Agronomy Department, University of Almeria, Almeria, Spain

[5] Research Centre for Scientific Collections from the University of Almeria (CECOUAL), 04120 Almería, Spain

[6] School of Mathematics, University of Minnesota, Minneapolis, MN 55455, USA

TROPOMI	TROPOspheric monitoring instrument
SEM–EDS	Scanning electron microscopy coupled with energy disperse spectrometer
TSP	Total suspended particles
UTC	Universal time conversion

1 Introduction

Aerosols originate both naturally or anthropogenically, and their composition, their effect on atmospheric processes and their physical and chemical properties are key components to understanding interactions with biogeochemical cycles that could affect rain and drought (Andreae 1995). Aerosol can be classified by sizing as: (a) fine mode particles corresponding to those with sizes < 1 µm, and (b) coarse mode particles with aerodynamic diameters > 2.5 µm and < 10 µm ($PM_{2.5–10}$) that vary from natural origin e.g., fungus, bacteria, pollen, or sea salt. Under natural conditions, fine particles, corresponding to the cloud condensation nuclei and ice nuclei, are suspended in the clouds and they may precipitate to the Earth's surface through raindrops in a process known as wet deposition (Seinfeld and Pandis 1998; Pöschl 2005). However, if no precipitation is present the concentration of airborne particle increases (Després et al. 2012; Fröhlich-Nowoisky et al. 2012). These airborne particles ultimately reach the Earth's surface through convective transport, diffusion, etc. (Pöschl 2005). Trade winds assist air masses to transport airborne particles longer distances, known as long range transport, which can occur through natural causes such as volcanic eruptions (Kahn and Limbacher 2012) and dust transport (Abdelkader et al. 2017; Di Biagio et al. 2017).

The main drivers affecting air quality and aerosol composition in cities stems from incomplete combustion during biomass burning, a common occurrence in many industries. For instance, biomass burning is usually considered one of the main culprits of deteriorated air quality (Ault et al. 2012; Zhang et al. 2014). While biomass burning is typically carried out in rural locations, the air quality of peri-urban areas can be altered by anthropogenic emissions as well. This may be due to the proximity between the countryside and big cities. This is more evident over those places with no buffering zones and that passing through an expansion of agriculture areas that promote biomass burning. Further potential factor affecting air quality is the high levels of smog (García-Franco 2020) and recurrent dust events from nearby deserts (Andreae et al. 2015; Soto-Coloballes 2020).

To understand South American air pollution in cities, Table 1 summarizes some relevant works conducted in selected cities in the region. These studies analyzed the concentration of both PM_{10} and $PM_{2.5}$ fractions. The concentrations found were related to conditions of human population, altitude, land use, and geographical position. For instance, early studies report that Cuenca, the third largest city in Ecuador, measures high daily particle concentrations of $PM_{2.5}$ (particulate matter < 2.5 µm) levels up to 30 µg m^{-3} (Astudillo-Alemán et al. 2015; Parra 2018). While in nearby cities such as Lima, Peru measure $PM_{2.5}$ concentrations of 26 µg m^{-3} which is accounted by the considerable number of industries in those regions (Silva et al. 2017). Hence,

Table 1 Summary of air quality among different cities in South America

City, Country	Lon, Lat	Avg. Population	Land use	Altitude (m asl)	Dates	Seasonality	Aerosol [µg m^{-3}]	
							PM_{10}	$PM_{2.5}$
Bogota, Colombia[a]	4° 36′ 57′′ N, 74° 08′ 37″ W	8 million	Urban	2600	Jul–Sep 2008	Dry season	55	NA
Cuenca, Ecuador[b]	2° 53′ 50′′ S, 79° 0′ 16″ W	0.5 million	Urban	2450	Jan–Apr 2013	Wet season	> 50	30
Lima, Peru[c]	12° 2′ 46′′ S, 77° 2′ 34″ W	> 10 million	Urban	500	2010–2014	Annual average	84	26
Quito, Ecuador[d]	0° 18′ 0′′ S, 78° 27′ 36″ W	2.2 million	Urban	2800	2007–2016	Annual average	> 26	> 17
Rio de Janeiro, Brazil[e]	22°54′30" S, 43° 11′ 47" W	6.6 million	Urban	40	2005–2011	Annual average	45	NA
Sao Paulo, Brazil[f]	23°33' S, 6° 38' W	20 million	Urban	760	1996–2011	Annual average	50	22

NA not available

[a]Vargas et al. (2012)

[b]Astudillo-Alemán et al. (2015), Parra (2018)

[c]Silva et al. (2017)

[d]Zalakeviciute et al. (2018b, 2020)

[e,f]Martins et al. (2017)

such levels pose a threat to those with sensitive respiratory systems (children and the elderly) which is corroborated by those findings carried out in a global context (Lelieveld et al. 2015).

Aerosol concentrations of PM_{10} are at high levels in cities like Rio de Janeiro and Sao Paulo, Brazil, which have a greater human population and major exchange markets (Martins et al. 2017), this is similar to Bogota, Colombia (Vargas et al. 2012). Recent studies on the effect of pollution in Andean populated cities, including Quito, revealed that environmental issues could be serious threats to human health (Bravo Alvarez et al. 2012; Cazorla 2016; Samek et al. 2018; Zalakeviciute et al. 2018a, 2020). One of the main forms of transportation in these Andean cities is the use of internal combustion (IC) engines. The atmospheric pressure in these cities is much lower (~ 15%) than the pressure at sea level (Zalakeviciute et al. 2018b). The IC engines operating in Andean cities are less efficient (as they were designed to operate at one atm), hence emitting greater amounts of hydrocarbons/PM than those IC engines operating at lower elevations (Bandowe et al. 2018).

Seasonality is a sub-analyze that is not common in Latin America urban pollution studies, as referred to in Table 1. There are many examples in northern hemisphere studies (Juneng et al. 2009; Hand et al. 2012); particularly due to the distinctive aerosol particle concentration during winter, spring, summer and autumn. Hence, this study will be focused on the intercomparison between wet and dry seasons which are common over the Tropical region.

The aim of the present study is (i) to provide a detailed characterization of ambient aerosol concentrations from total suspended particles (TSP), PM_{10}, $PM_{2.5}$ and PM_1 based on 14 months of continuous monitoring in the city of Guayaquil, Ecuador; (ii) to relate the spatial and temporal patterns to meteorological conditions of the city; and (iii) to conduct fine/coarse particle morphology and determine the chemical composition of PM collected at various sampling locations. The present work is mainly focused on particulate matter and not on other pollution traces.

2 Methodology

2.1 Study Area and Instrumentation

Guayaquil is a coastal city located in the southwest sector of Ecuador at 4 m asl with approximately 3 million inhabitants. It is one of the most populated cities in Ecuador and its major industry is international trade due to its harbor located at the end of the gulf of Guayaquil with an estimated area of 344.5 km^2 (Delgado 2013). The exponential growth of the city's population and trade market have made it a congested urban city with significant environmental threats (Rissler et al. 2014; Zalakeviciute et al. 2020). However, there are surprisingly few objective studies on the environmental effects and pollution stemming from population growth and rise in industry. During the early 1990's, an external consulting company, Espey & Houston Inc-COPADE, prepared the first report regarding the air quality of the city. The report defined hotspots from north to south and reported an estimated of 50 μg m^{-3} with heavy concentrations over the industrial site "Isla Trinitaria" due to electric power plants at the time (Borbor and Barriga 2007). In addition, several local studies from 2000 and 2016 reported values of PM_{10} at approximately 50 μg m^{-3} (Eficacitas 2007) and of $PM_{2.5}$ at ~ 25 μg m^{-3} (FLACSO et al. 2008).

The geographical location of the studied area is located at: 2° 10′ 2.1″ S, 79° 53′ 29.93′ W at 10 m asl; in which ambient aerosols were measured with a dust particle counter that was located outside a storage cellar. The data was accessed online from the AirQweb 2018 website (https://www.airqweb.com/Main, last visited on June 20, 2018). Initially, the data were gathered using an external particle counter TOPAS from Turnkey Instruments (Cheshire UK from LATAN) installed from September 1, 2015 to November 17, 2016 UTC-5, with 10-min time resolution. The instrument allows the measurement of TSP and mass concentrations up to 6000 μg m^{-3}, PM_{10}, $PM_{2.5}$ and PM_1; the relevant online data is summarized and presented in Table 2. Due to the fact that the TOPAS instrument went to maintenance and it was put offline on November 17 at 17:50 (UTC-5), the TOPAS was replaced with a new particle counter, Dylos DC1100 with PC interface (Gramsch et al. 2020). The performance of the low-cost aerosol sensor (Dylos DC1100) compared to the TOPAS instrument was adequately validated prior to the data collection. The intercomparison between TOPAS and Dylos DC1100 is presented in a graphic (included as supplementary S1 material) and it shows an acceptable correlation. Other researchers have reported the evaluation of the low-cost monitoring (Dylos) with more expensive instruments and correlation with similar results (Steinle et al. 2015; Vercellino et al. 2018).

2.2 Meteorological Conditions

Meteorological data were collected using the ESPOL Lab-FREE project (2008–2015) which consist on HOBO weather station with the following items: Temperature/RH smart sensor (S-THB-M00x, temperature working range − 40° to 75° C with ± 2.5% °C, RH > 95% increased 1% error), rain gauge smart sensor (S-RGA-M002, accuracy ± 1% at up to 20 mm/h, wind direction smart sensor (S-WDA-M003, accuracy ± 5°), wind speed smart sensor (S-WSA-M003, accuracy ± 1.1 m/s) and a HOBO U30 cellular data logger U30-GSM. As a reference, weather data from the Instituto Oceanográfico de la Armada of Ecuador INOCAR, that have

Table 2 Descriptive statistic of ambient aerosol TSP, PM_{10}, $PM_{2.5}$ and PM_1 minimum, mean and maximum data from September 2015 to November 2016 at Guayaquil monitoring station, where values within square brackets represent periods with gap data

		TSP [μg m^{-3}]				PM_{10} [μg m^{-3}]				$PM_{2.5}$ [μg m^{-3}]				PM_1 [μg m^{-3}]			
Year	Month	Min.	Mean	SD	Max.	Min.	Mean	SD	Max.	Min.	Mean	SD	Max.	Min.	Mean	SD	Max
2015	Sep	10.6	31.9	10.5	132.6	6.3	20.9	6.9	80.6	2.1	6.2	2.1	17.8	0.3	1.1	0.4	2.7
	Oct*	[13.5]	[36.6]	[12.1]	[210.4]	[7.9]	[24.3]	[7.8]	[118.3]	[2.9]	[7.5]	[2.8]	[25.6]	[0.3]	[1.3]	[0.6]	[7.3]
	Nov	14.6	36.6	13.1	223.0	10.0	25.1	8.4	154.6	3.3	8.5	2.5	18.4	0.5	1.5	0.5	3.7
	Dec	11.0	31.2	12.1	211.3	6.6	21.0	7.5	153.0	2.1	6.8	2.0	24.4	0.2	1.1	0.4	4.1
2016	Jan*	[6.6]	[34.1]	[14.1]	[172.6]	[5.3]	[22.2]	[8.4]	[113.7]	[0.8]	[6.0]	[2.2]	[32.4]	[0.2]	[1.0]	[0.5]	[10.9]
	Feb	4.4	31.1	15.1	128.6	2.6	20.5	9.7	78.1	0.9	5.6	2.2	21.0	0.1	0.9	0.4	6.2
	Mar	3.6	29.9	17.2	181.4	1.6	18.4	9.6	97.7	0.4	4.6	1.9	16.3	0.0	0.9	0.4	5.2
	Apr	4.2	31.8	30.9	162.0	2.6	20.7	17.8	104.7	0.8	5.8	3.1	23.4	0.1	1.1	0.6	8.3
	May	11.4	34.3	14.4	252.1	5.7	22.4	8.9	162.4	1.9	6.6	2.4	26.1	0.3	1.2	0.5	8.2
	Jun	10.5	35.1	14.2	275.1	7.0	23.8	9.2	195.5	2.5	7.7	2.6	41.3	0.3	1.4	0.5	11.7
	Jul	10.7	30.8	12.1	106.8	5.7	21.3	7.8	61.6	1.7	7.2	2.5	28.3	0.3	1.3	0.6	8.9
	Aug	8.3	28.7	10.5	88.7	3.9	20.0	6.8	60.3	1.3	7.5	2.6	19.0	0.0	1.4	0.5	6.5
	Sep	7.6	25.6	12.2	122.4	4.9	17.6	7.8	80.3	2.1	6.3	2.8	37.5	0.0	1.3	0.7	11.4
	Oct	7.3	29.8	10.4	237.8	3.3	20.7	6.7	173.6	1.2	7.6	2.3	16.1	0.1	1.4	0.5	5.5
	Nov*	[12.1]	[33.7]	[12.1]	[135.4]	[8.9]	[21.9]	[6.4]	[105.0]	[2.6]	[7.2]	[2.1]	[21.5]	[0.5]	[1.4]	[0.8]	[7.8]
Annual	avg	8.7	31.4	14.4	176.8	5.0	21.0	8.9	116.9	1.7	6.7	2.4	24.1	0.2	1.2	0.5	6.9

Wet season (Jan–May, in blue color), dry season (Aug–Nov, in orange color) and transition season in white, as presented in Fig. 1

accessible online data to (https://www.inocar.mil.ec/web/index.php/precipitacion-en-guayaquil, last visited on June 2018), and the weather stations from Benemérito Cuerpo de Bomberos de Guayaquil from 2016 to 2018.

Guayaquil weather correspond to the tropical savanna climate (Aw) corresponding to the Köppen climate classification; in which, mean temperature fluctuated from 23° to 26 °C and annual precipitation rate from 500 to 1000 mm and it varies from year to year. The seasonality split on two seasons: the wet season runs from the end of December to May and the dry season runs from July until November while December and June are considered as transitional periods. Annual seasonality has been characterized by many authors (Cañadas Cruz 1983; García-Garizábal 2017) to be due to trade winds related to the cold Humboldt current that converge near the equatorial. These periods may differ each year, but the trend patterns seem to remain consistent (Thiel et al. 2007).

2.3 Air Masses Trajectory Analysis

Air mass characterization was conducted using Hybrid Single Particle Lagrangian Integrated Trajectory (HYSPLIT) (Stein et al. 2015; Draxler et al. 2018) in which the air counter location was taken as the starting point and with historical data from January 1, 2015 to December 31, 2017. Using a combination of air mass studies encompassing a 96 h backward trajectory at a 200 m height above ground level (https://ready.arl.noaa.gov/hypub-bin/trajtype.pl?runtype=archive) and a georeferenced list of the areas being studied (e.g. mining, industry, energy and water infrastructure), we were able to identify pollution hot-spots and emission sources, which can be compared to determine how the region is affected by different industries. Using this data, we have been able to identify how industrial pollution is translocated to Guayaquil.

Anthropogenic activities such as: burning fuel, vehicle emissions, power plants and others are among the different sources of NO_2 (Seinfeld and Pandis 1998). It is believed that higher NO_2 concentrations play a crucial role of anthropogenic sources. A remote atmospheric sounding instrument (TROPOspheric Monitoring Instrument, TROPOMI) that provide spatial continuous information of the earth surface at a daily scale, was used to survey air pollution of the city. We use the OMI Total Vertical Column NO_2 product with level-2 NRTI:2018-10-24 (http://www.tropomi.eu/data-products/nitrogen-dioxide) last visited on 22 July 2020. The selected periods (Aug–Nov 2018; Aug–Nov 2019) were averaged daily map tiles for the dry season and selected periods (Jan–May 2019) were averaged daily map tiles for the wet season. The methodology used in our work closely follows the published works by other researchers (Krotkov et al. 2017; Zhao et al. 2020).

Additionally, some products from NASA Giovanni (Geospatial Interactive Online Visualization and Analyze Infrastructure) (Acker et al. 2014; Luna et al. 2018) web server were used to visualize aerosol presence, in which there were: (i) Aerosol Optical Depth at 550 nm (AOD_{550nm}) at a wavelength of 550 nm from the moderate resolution imaging spectroradiometers (MODIS) on the satellites Terra and Aqua combined dark target deep blue AOD products (MOD08_D3_V6_ and (MYD08_D3_v6), and (ii) Tropical Rainfall Measurement Mission TRMM (TRM_3B42_Daily_v7 product), (https://giovanni.gsfc.nasa.gov/giovanni/), last visited on May 15 2018.

2.4 Sampling and Microscopy Analysis

Carbon membranes (disk of 12-mm diameter, brand Agar Scientific) were placed at three selected locations: (a) outside the city, (b) residential area and (c) city center. The sampling locations were uniquely selected as to represent the various types of airborne particle matters. Thus, the sampling encompassed a heavy-duty truck highway or the "highway to via costa" outside of the city, a residential area that is highly populated, and the final selected sampling location is city center or the "Archivo Historico". The wet season in Guayaquil is composed of heavy rains (precipitation or ~ 200 mm per month), flooding, high humidity (RH > 80%) and other related issues. Therefore, due to climate conditions the collection of samples during the wet season is not as practical as during the dry season. Additionally, the interpretation of samples collected during the wet season can be difficult and a good assessment may require an analysis (physical and chemically) of rainwater samples for comparison (Holecek et al. 2007). Due to the complexity of the wet season, only one location was considered. This location is named "Colon". The location was selected because of being in the vicinity of the TOPAS. City center is heavily trafficked by people, taxis, small passenger vehicles, etc.; and it is close to the airport cellar measurement station. During the sampling, carbon membranes were left for approximately 4–7 days in open environments of the selected locations, refer to Fig. 4c and Table 3. The carbon membrane disks were placed at 2 m height above the ground, facing SW winds and with a cover protection over the border.

After the samples were collected, they were kept isolated in a cold environment at 7 °C in a refrigeration unit. Collected aerosol samples were exposed to gold sputtering for 120 s to render them stable under the electron microscope beam. The FEI-SEM with an integrated energy spectrometry (EDS) was used to study the chemical composition of selected samples using Genesis spectrum software (Baron and Willeke 2001; EDAX 2006). The methodology for chemical characterization of ambient aerosols by Moffet (2011), Burkhardt (2010) mentioned that SEM techniques are good for certain elements but not constituent (e.g. carbon, nitrogen), fine and coarse morphology. The SEM images were analyzed at a working distance of 10 mm, the detectors used were: Everhart–Thornley detector ETD and Back Scattering Electron Detector BSED with magnifications of: 3000x, 12,000 × until 100,000x; while performing EDS analysis, all analysis were taken by point to point to the sample on the surface of a selected structure. Elements like Au and Pd are considered traces of the gold sputtering. The sampling methodology on the collection of particles was conducted following closely the work in the literature (Morillas et al. 2016).

The data analysis was performed using the software Dylos Logger version 3.1.0, and R program version R 3.5.1 coupled with rstudio and packages openair, maps, maptools (Carslaw and Ropkins 2012; Carslaw and Beevers 2013; Grange et al. 2016) and Igor pro version 6.3.7 map script templates (Pöhlker et al. 2019) and ArcView for maps and data analysis and plotting (Zhao et al. 2020).

3 Results and Discussion

3.1 Meteorological Conditions and Particle Concentrations

Meteorological data showed that the wet season of 2016 received a cumulative precipitation of 1000 mm of rain (Fig. 1a). The majority of rainfall occurring in the first quarter of the year January to April, while the dry season ranged from August to November. Besides, certain months such as May, June, July and December are transitional months when sporadic rain episodes may occur. Average temperatures during the wet season and mean relative humidity (RH) of 27 °C and 78% occurred, while during the dry season, temperatures dropped to 24 °C with a mean RH of 73%, refer to Fig. 1b, c. As shown in Fig. 1a, the presented data agree with previous findings from Cañadas Cruz (1983); in which the tropical weather in the coast of Ecuador is described.

Average wind speed during the daytime were 1 m s^{-1} during the wet season and increased to 2 m s^{-1} during the dry season, while nighttime average wind speeds were maintained at 1 m s^{-1} during the wet season and rose to 3 m s^{-1} (approximately two folds higher) during the dry season

Table 3 Descriptive statistic of $PM_{2.5}$, location and weather conditions during the sampling period

	Time (YYYY-MM-DD HH:MM)		$PM_{2.5}$ [μg m^{-3}]			Temperature [°C]			RH [%]			Rainfall [mm day^{-1}]
Location	Start	End	Min	Mean	Max	Min	Mean	Max	Min	Mean	Max	
Residential	2018–10-22 14:00	2018–10-29 14:00	0.5	11.2	80.8	21.0	24.2	31.8	51.0	74.5	88.0	0
Outside city	2018–11-09 11:30	2018–11-12 11:30	2.7	9.7	37.0	22.7	25.5	33.1	52.0	74.3	86.0	0.5
City center	2018–11-30 11:30	2018–12-07 11:30	1.0	11.8	80.0	21.1	24.7	31.7	49.0	71.5	86.0	0.2
City center	2019–03-02 18:00	2019–03-16 11:30	[2.0]	[7.9]	[23.5]	23.1	27.3	34.2	54.0	82.8	97.0	79

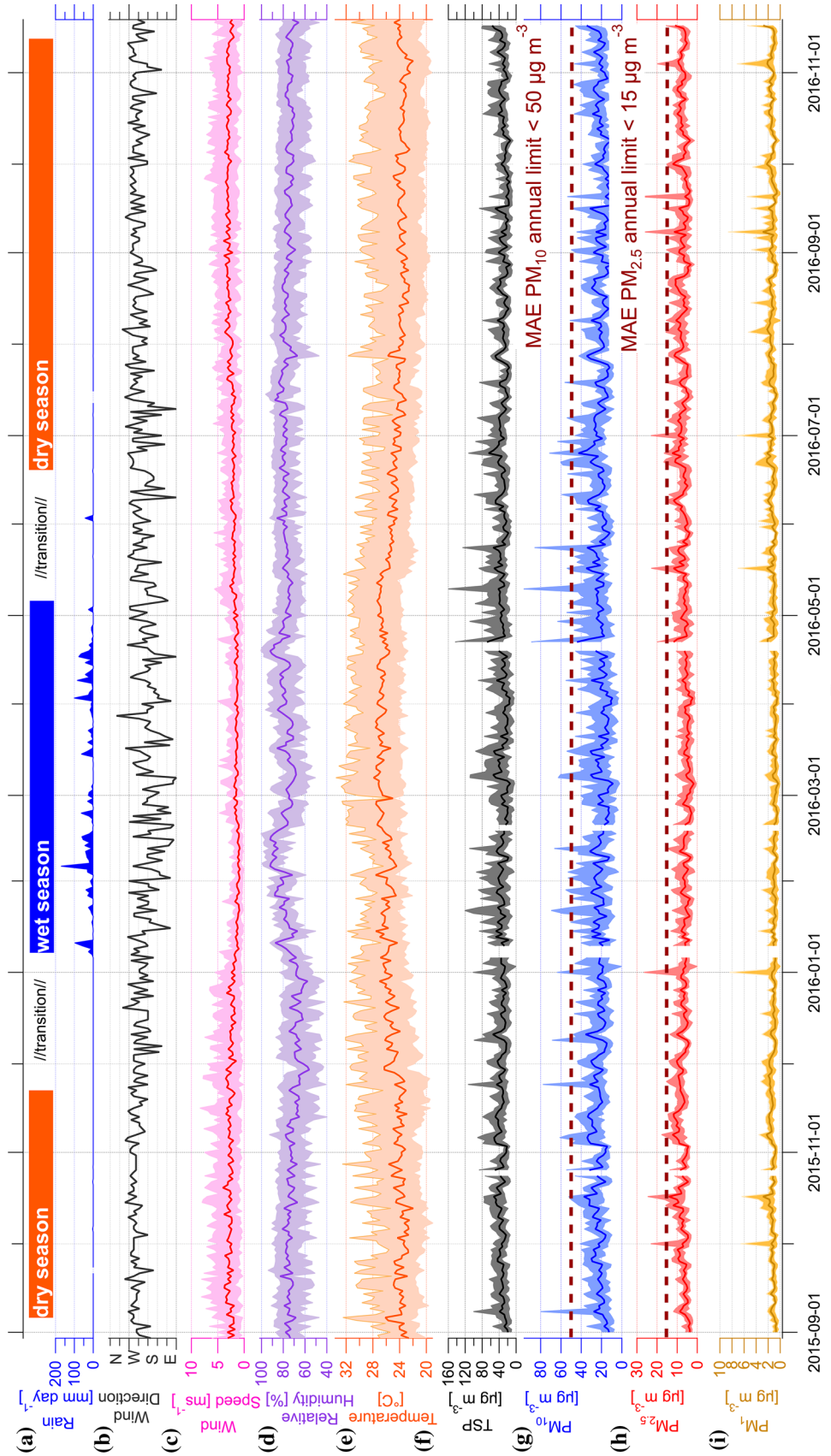

Fig. 1 Meteorological conditions of **a** rainfall, **b** wind direction, **c** wind speed, **d** relative humidity, **e** temperature data from northwest of Guayaquil daily averages with wet season (January–May) and dry season (July–November) and June and December as transitional periods, and **f** total suspended particles TSP, **g** PM_{10}, **h** $PM_{2.5}$ and **i** PM_1 daily averages in Guayaquil. Red dashed line represents maximum PM_{10} allowed after 12-month continuous monitoring according to MAE

(Fig. 1b, c). In regards of the wind direction, it showed a continuous path from south and south-west wind throughout the year. There are some occasional periods during the daytime, when winds from the north when wind speed remained quiet low (< 1 m s^{-1}).

During the rainy season, most of the large particles, particularly those of TSP and PM_{10} were affected due to wet deposition, when rain helps TSP and PM precipitate to the ground rather than remain floating in the air (Pöschl 2005; Zalakeviciute et al. 2018a; Zhou et al. 2020). This effect is mainly noticeable with averaged values about 30 µg m^{-3} for TSP and 20 µg m^{-3} for PM_{10}, respectively. Nonetheless, the concentrations of TSP and PM_{10} sporadically spikes during the absence of rain Fig. 1a, f, and g and Table 2; in which values peak to 160 µg m^{-3} for TSP and 98 µg m^{-3} for PM_{10}, respectively. Regarding $PM_{2.5}$ and PM_1 were at about 6 µg m^{-3} for $PM_{2.5}$ and 1 µg m^{-3} for PM_1. Nonetheless, sporadic spikes in $PM_{2.5}$ and PM_1 can be found the whole year, no matter the seasonality, see Fig. 1a, h and i and Table 2; in which values peaked to 23 µg m^{-3} for $PM_{2.5}$ and 8 µg m^{-3} for PM_1.

In contrast, during the dry season for TSP and PM_{10}, Fig. 1a, f and g and Table 2, shows averaged values about 29 µg m^{-3} for TSP and 20 µg m^{-3} for PM_{10}, respectively. Meanwhile, sporadic spikes in TSP and PM_{10} can be found during the absence of rain during the dry season with peaked values of 140 µg m^{-3} for TSP and 93 µg m^{-3} for PM_{10}. The average concentrations of $PM_{2.5}$ and PM_1, Fig. 1a, h and i and Table 2, are 7 µg m^{-3} for $PM_{2.5}$ and 1 µg m^{-3} for PM_1. Meanwhile, there are sporadic spikes in $PM_{2.5}$ and PM_1 and they take place mostly during the dry season with peaked values. Moreover, there are higher wind speeds and variations of wind direction, refer to Fig. 1b, c, during the dry season rather than the wet season, which may contribute to the transport of PM during the dry season.

According to the Ministry of Environment in Ecuador MAE air quality norm Book IV Annexes 3 and 3a, annual average PM_{10} should not exceed 50 µg m^{-3}, while the reported data are 21 µg m^{-3} for the whole year (Table 2). $PM_{2.5}$ should not exceed 15 µg m^{-3} during a 24 h continuous measurement, while the reported data show 7 µg m^{-3} for the whole year. Furthermore, the maximum values reported show higher numbers particularly for the months of June and October of 2016 for PM_{10} with values of 195 µg m^{-3} and 173 µg m^{-3}, respectively. Within the months of June and September of 2016 for $PM_{2.5}$ with values of 41 µg m^{-3} and 37 µg m^{-3}, respectively. Diurnal average data reveal that higher peaks tend to become more frequent in the afternoon and night times, refer to Fig. 2d, f. The windy season in Guayaquil starts on the second half of the year, while the windiest months in Guayaquil occurs from August to November (Johansson et al. 2018). According with our data, the average wind speed in February is 1 m s^{-1} while in September is 3 m s^{-1}; throughout the year, the increase of the wind occurs in the afternoons around 14:00–18:00 and gradually increased until midnight. Seasonality plays a key role in here because high wind speed transport pollution during the dry season. Therefore, our study suggest that this may correspond to the double high peaks particularly during the dry months, refer to Figure Supplementary S2. In regards of the wind directions, some studies suggested that higher $PM_{2.5}$ concentrations at night occur due the decrease of the planetary boundary layer; and consequently, enhance the presence of pollution in the air of megacities (Gago et al. 2013; Miao et al. 2019). According with Seinfeld and Pandis (1998) those events occur under lower temperatures at night and under steady wind speed conditions. In contrast, our study shows high wind speed events during the night (refer to Figure Supplement S2) no matter the seasonality. Thus, we imply the high PM concentration peaks are due to long-range transport events from the south gulf path. Moreover, it is important to remark that there is no mandatory reference in regards of TSP or PM_1; nonetheless, those values are also reported in Table 2 as reference.

Diurnal cycles of PM show that PM_{10} and $PM_{2.5}$ average values are below those limits set by MAE air quality norm Book IV Annexes 3 and 3a. However, while considering the minimum and maximum data fluctuated substantially in all cases (TSP, PM_{10}, $PM_{2.5}$ and PM_1) in terms of annual and seasonal occurrence, the collected data of aerosol particulates during the wet and dry season show a bimodal shape with a very prominent peak at 7:00–9:00, mainly for TSP and PM_{10} during the wet season, refer to Fig. 2a, c. Thus, for $PM_{2.5}$ and PM_1 average concentrations, there are no distinguished peaks, rather small humps from mornings and afternoons, refer to Fig. 2e, g. In contrast, considering the minimum and maximum values during the dry season, the morning peak is shifted towards 10:00–11:00 h for TSP and PM_{10}. A second peak occurs at 14:00–17:00 h for all particle size TSP, PM_{10}, $PM_{2.5}$ and PM_1 during the dry season, refer to Fig. 2a–d.

Hence, regardless of the season (wet/dry), the average values of PM_{10} and $PM_{2.5}$ between 6:00 and 10:00 rise closer to the MAE limit; most likely due to the morning urban traffic no matter the seasonality, similar situations have been found by (Martins et al. 2017) studies at certain urban areas in Brazil and by in Quito (Zalakeviciute et al. 2018b); mainly during the wet season.

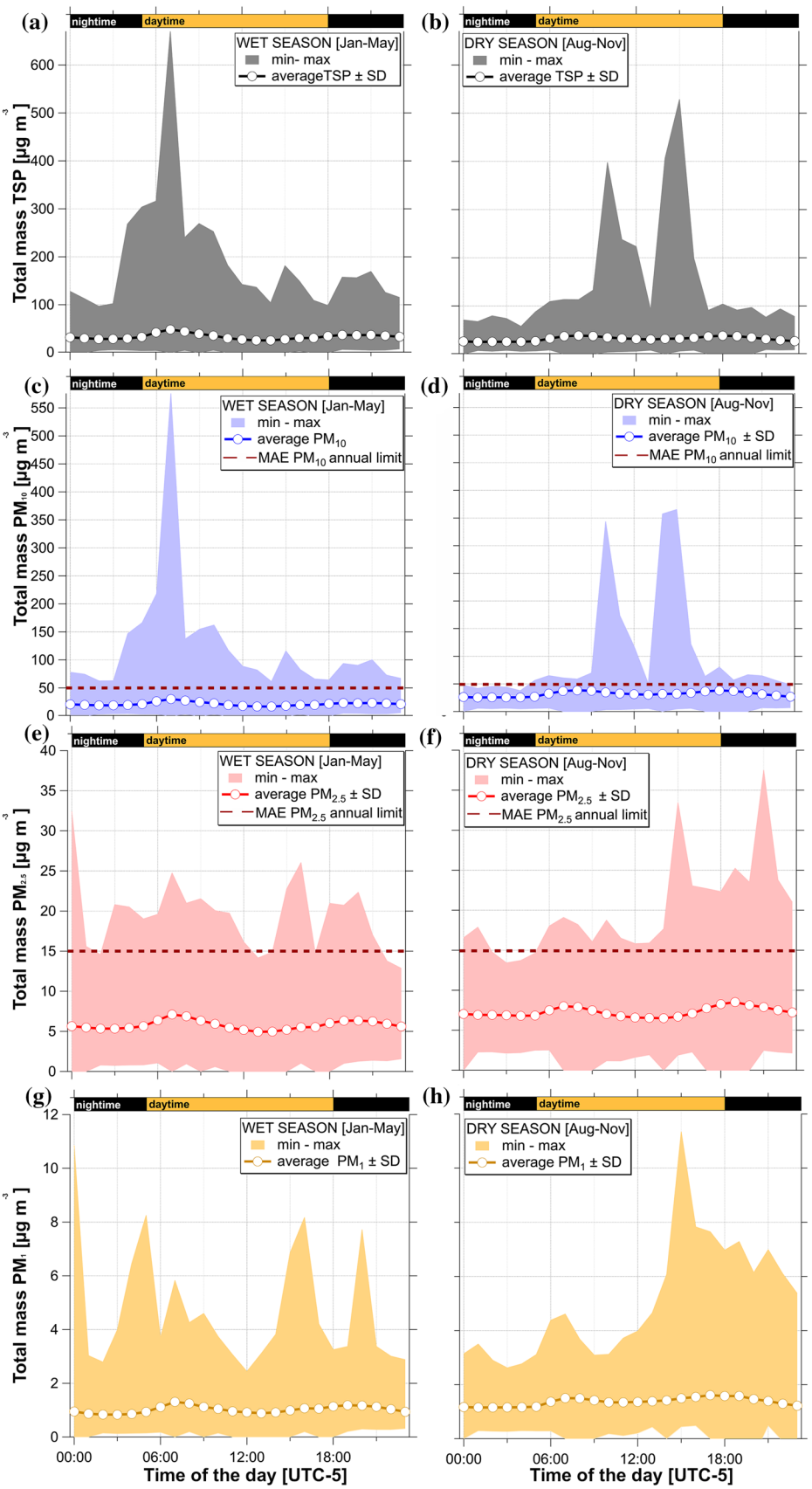

Fig. 2 Diurnal cycle of: **a** TSP, **c** PM_{10}, **e** $PM_{2.5}$, and **g** PM_1 from January to May 2016 and **b** TSP, **d** PM_{10}, **f** $PM_{2.5}$ and **h** PM_1 from September to November 2015 and July to November 2016 at Guayaquil monitoring station

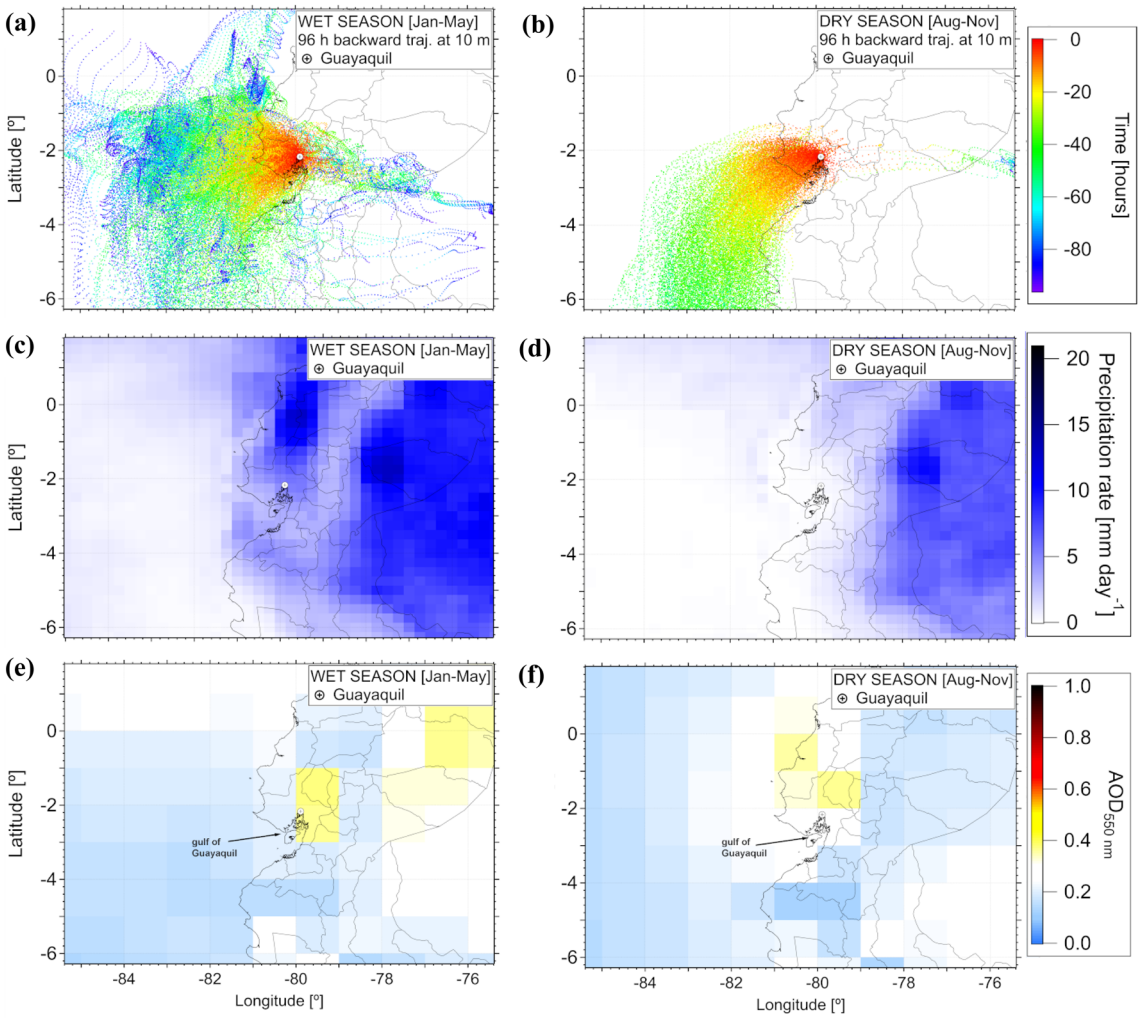

Fig. 3 Annual air masses reaching Guayaquil: **a** typical air masses occurrences during the wet season, **b** 2015 AOD 550 MODIS combine Terra/aqua during the wet season, **c** typical air masses occurrences during the dry season, and **d** 2015 AOD 550 MODIS combine Terra/aqua during the dry season

3.2 Backward Trajectories Analysis, Seasonality and NO_2

Backward trajectories of air masses analysis showed that during the wet season, there is an influx of air masses. Thus, air masses follow the trajectory from the gulf of Guayaquil, as well as the Guayas River, which steers air masses from south towards the north until reaching continental inland (Fig. 3a). During the dry season, air masses become south and south-west dominant (Fig. 3b). Besides, the precipitation rates during the wet season (see Fig. 3c) are prominent particularly in the coastland and shows a remarkable contrast to the dry season, as presented and correlated with the data presented in Fig. 1a.

There is an absence of strong winds during the wet season; in contrast, south and south-west winds are strong during the dry season. This can be observed in Fig. 1b, c, respectively.

Furthermore, the aerosol Optical Depth (AOD) shows the presence of aerosol in the atmosphere during the wet season and it shows a footprint of aerosol particle suspended in the air which fades out during the dry seasons. Despite the fact of high incidence of aerosol particles along the trajectory during the wet season, most PM are scavenged due to wet deposition before reaching the city (Fig. 3c, d) and Fig. 1a. Thus, higher aerosol peaks are seen during the absence of rain and increase in temperature, particularly during heavy traffic hours (07:00 in the mornings and 16:00 in the afternoons, UTC-5). Consequently, if there is more PM during the dry season it may be produced by two effects: (a) long range transport from south/west locations and (b) from the background urban pollution.

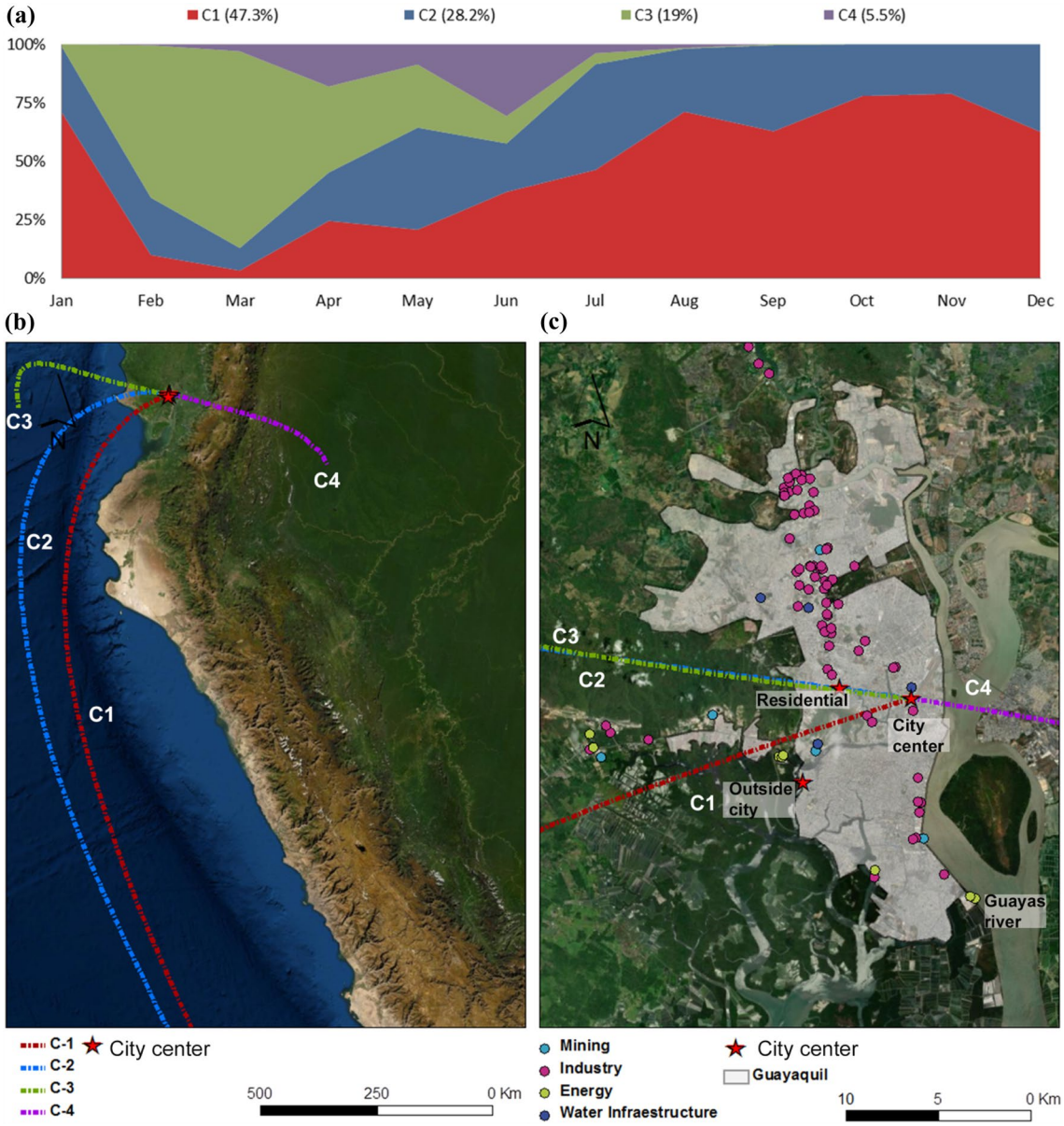

Fig. 4 Cluster analysis of backward trajectories from 2015 and 2016 and main contamination emission sources from Guayaquil

The PM shown during the period 2015–2016 may correspond to Guayaquil's unique geographical conditions. During the wet season, the city experiences more regional pollution, while during the dry season, it may experience long range transport in addition to its local pollution. Similar findings agree with pollution and wind relationship as mentioned by Wang and Ogawa (2015) in Japan. Thus, we observe that any sign of external contamination may be occurring when strong winds increase (e.g. > 3 m s^{-1}); possibly transporting external $PM_{2.5}$ and PM_1 from south and south west sources. The higher wind speeds and directions correlate well with the geographical location of the city, which is located on the west bank of a large river flowing into the gulf and finally into the Pacific Ocean. Ecuador's main port is located at the southern part of Guayaquil.

A cluster classification of all trajectories occurred from 2015 to 2016 showed four main paths along with their respective contribution: C1 (47%), C2 (28%), C3 (19%) and C4 (6%). The three main sources correspond to south (red dashed line, C1), southwest (blue dashed line, C2), west regions (green dashed line, C3) and east regions (purple dashed line, C4), refer to Fig. 4a, b. Thus, a temporal analysis shows the C1 and C2 are mainly occurring the whole year, while C3 and C4 are most common during the wet season.

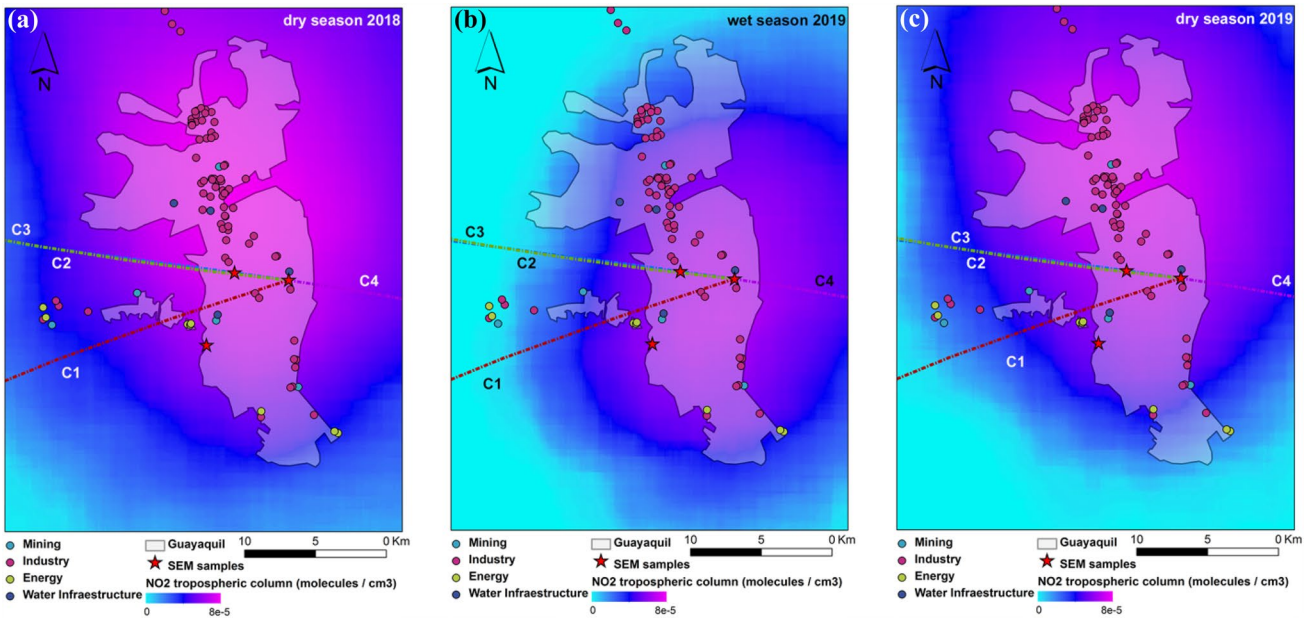

Fig. 5 Guayaquil NO_2 map **a** dry season 2018 (Aug–Nov), **b** wet season 2019 (Jan–May 2019), and **c** dry season 2019 (Aug–Nov 2019). Main contamination emission sources and clusters solution

Main anthropogenic activities such as: mining, energy and water infrastructure, are located at the south and north of the city, while mining and energy, are both located at the west of the north of peri-urban area of the city, as presented in Figs. 4c/5a–c.

It seems that using the total vertical column of NO_2 as pollutant tracer, it sums up the local pollution during the dry season, refer to Fig. 5a, c, while during the wet season, pollution is mainly concentrated on the city center, refer to Fig. 5b. These findings correlate well with previously data presented in Fig. 2 (PM seasonality) and figure supplement S2. Total NO_2 column during the wet season, refer to Fig. 5b, shows an increase of the pollution spectrum from the north and northeast. The reason of this may be due to that most industries, energy and mining activities are concentrated nearby. They coincide with the cluster analysis C1, C2 and C3, which contribute with 94% of the air masses throughout the year. Consequently, part of those anthropogenic activities could be reflected as part of the pollution transport into the city center particularly at nighttime, according to Fig. 5c.

These trends are presented as guidance to understand critical pollution hotspot in the city. As previously presented by Zhao et al. (2020), total NO_2 column data are more precise over rural areas rather than urban and suburban areas in Canada in the city of Toronto. Moreover, ground measurements carried out by Cazorla (2016) in Ecuador in the city of Quito, showed low ozone and NO_x levels during three months measurements from July to September, emphasizing that pollution ratio may imply further complex interactions at least for high altitude cities like in Quito at 2800 m asl.

Although the data presented provide good information of airborne particle concentrations within the city, this does not answer the question of the morphology and characteristics of the ambient particles found. To provide insight about the morphology and main characteristics of aerosol particles, some samples were taken during the dry season of 2018.

3.3 Morphology of Aerosol Particles During the Dry Season

The sampling period during the dry season of 2018 shows $PM_{2.5}$ concentrations of 9, 11 and 12 μg m^{-3} from outside the city, residential area and city center, respectively, refer to Table 3. Hence, these areas were selected for placing the carbon membranes for collecting the physical samples. Regarding the morphological characteristics the samples shown in Fig. 6a1–a3 are from the residential area; Fig. 6b1–b3 represents characteristics of samples collected from outside the city; and Fig. 6c, d shows samples collected from the city center. The low-resolution SEM images of lighter contrast (Fig. 6c1) represent processed raw SEM images to assist in visualization and comparison of the density of the "*as-trapped*" airborne PM present at the various studied locations. Higher resolution (HR) SEM and SEM–EDS analysis show that the structural morphology and chemical constituents of these urban dusts are quite complex and vary with location.

SEM imaging shows that the dust samples are composed of very irregular shaped or anomalous structures, some have sharp-edges (dotted arrows in Fig. 6a2), as well

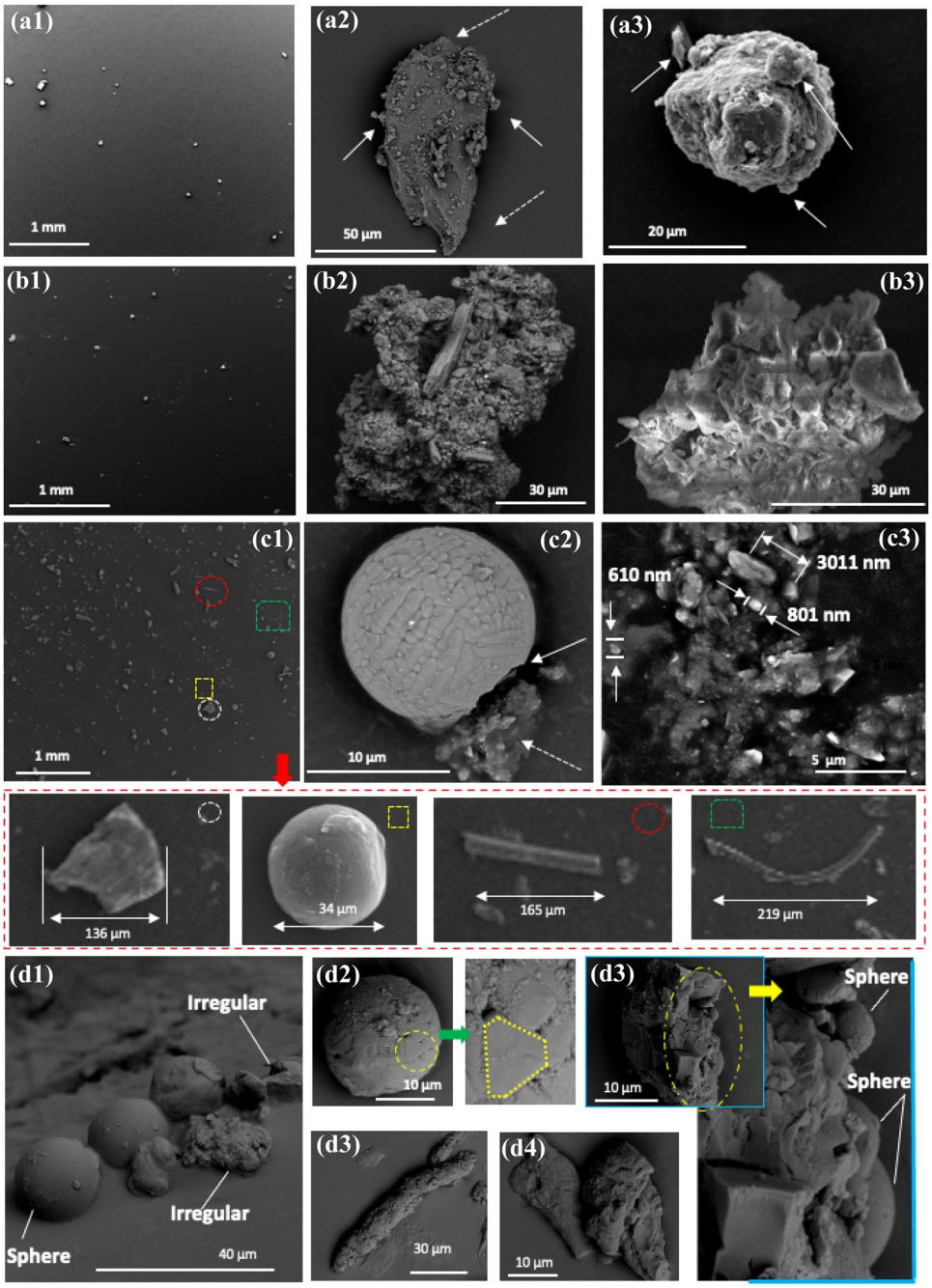

Fig. 6 **a1**-**a3** Represents lower resolution SEM images of the "as-trapped" airborne PM after being strike on carbon tapes placed in open conditions from the residential area; **b1**–**b3** from outside city; **c1**–**c3** city center and **d1**–**d6** city center during the wet season. The urban dust of Guayaquil city center appears to be composed an aerosol of a polydisperse size distribution and varying shapes (magnified view 1–4)

as structures with much more well-defined shapes such as spherical or rod-like morphologies. Some of the dust particles appear to be composed of a collection or aggregates of smaller shapeless particles (Fig. 6b2, b3), while others appear to be composed of relatively larger solid angular and shapeless particles with a coarse surface texture having a high density of smaller particles attached to their surface (as highlighted with the solid arrows in Fig. 6a2, a3. The particle in Fig. 6a3) has a coarse-grained porous texture. The urban dust present in the city downtown area appears to be composed of particles with a variety of shapes and of a polydisperse size distribution (Fig. 6c1). The urban dust in Fig. 6c1 is composed of relatively large and sharp-edged (magnified view 1), spheroidal-shape particles (inmagnified view 2), straight and axial elongated rod-like structures (magnified view 3) and fiber-like with a radius of gyration (magnified view 4). The spherule in Fig. 6c2 is a "close-up" view of one of the smaller structures in Fig. 6c1. The spheroidal has a small fracture on its surface (solid arrow) revealing that the particle was formed of a collection of smaller shapeless dust particles (dotted arrow). However, the surface of the spheroidal is

rather smooth and does not contain deposition or absorbed materials attached to its surface as seen present in the samples collected in the residential area Fig. 6a2, a3. The HR-SEM shows submicron scaled particles form the larger structures Fig. 6c3. Figure 6d1–d5 represents SEM images collected on the surface of sample collectors positioned in the city center during the wet season. Figure 6d1 shows that large spherical shape structures are surrounded by other large irregular-in-shape structures. Higher resolution SEM imaging of the nearly spherical and irregular structures are shown in Fig. 6d2–d4. A higher resolution SEM analysis on a typical circular structure shows that its surface contains smaller irregular-in-shape deposits. Additionally, a closeup view on surface areas of the sphere where there is not accumulation of deposits show that the spherical particles have a very peculiar structure. It appears that the spherical structure is formed of smaller independent structures as shown by the presence of grain-like boundaries along the surface of the sphere (inset of Fig. 6d2). It is interesting to note that spherical structure that the spherical structure of the dry sample (Fig. 6c2) appears to have a similar morphology. SEM imaging analysis also show that some of the wet deposits are composed of large irregular and spherical like structures (Fig. 6d5). The inset of Fig. 6d5 shows the spherical structures of various diameters at the bottom of the cluster.

The localized pollution in Guayaquil is considered to be at a safe level by governmental mandated standards (MAE 2011). The reason for such safe levels of pollution is likely related to the unique geographical location of the city, which is surrounded by the gulf of Guayaquil and estuaries (Pinto and Slowey 2021), as well as some hills < 500 m in height with smooth slopes, refer to Fig. 4b, c. In contrast, wind coming from the Pacific Ocean, particularly during the dry season, may contribute to the long-range transport of pollutants to the most eastern parts of the city.

Single particle chemical analysis of the capture particles differ from their location; in which: (a) residential samples show high trace of N, Na, S, Ca, Si and Al; (b) city center samples show trace of N, Na, Mo, Ca during the dry season; (c) outside the city shows trace of Na, Mg, Al, Si, Ca and Fe, and d) N, Na, Fe, Mg, Al, during the wet season, refer to Figure Supplementary S3. Chemical elements like: C, Au and Pd correspond to the sampling methodology of the carbon pin and the gold sputtering. Na, Ca and S were the dominant elements found in most of the samples regardless the location and due to the size and their morphology we infer they can be some traces of anthropogenic emissions (e.g. urban dust, soil and industries). In that regards, similar findings agree which compare urban and rural areas in the Mediterranean area (Morillas et al. 2016; Genga et al. 2018; Perrone et al. 2018); in Poland by Samek et al. (2018); and in Quito, Ecuador by Zalakeviciute et al. (2020). Besides, sea salt aging plus the urban pollution of the city was found in Macao by Li et al. (2011) with traces of N, O, Na and S were found in certain samples at the residential areas and downtown below $PM_{2.5}$; our findings present similar pattern at certain locations but at particles corresponding to coarse mode PM_{10} mostly.

Dust particles can be characterized by their unique surface morphology. It has been suggested that dust particles can have two exclusive and often coexisting types of surface roughness. One type is that the particle surface itself can be rough, while in the other type, the roughness is created by natural deposition or agglomeration of small particles on the surface of the large dust particle (Nousiainen 2009). In the context of particle morphology, dust particles are not spherical or nearly spherical, rather they have a very irregular shape and structure (Nousiainen 2009). The morphology (shape and size) of some of our structures resemble dust particles. Dust particles can have a variety of shapes, compactness, and be formed of mixtures of different mineral species (most notably birefringent) (Nousiainen 2009). Particles released from biomass burning or incomplete combustion have a nearly spherical shape and are composed mostly of carbon and oxygen (Chou et al. 2008); among other elements as: Ca-rich, Fe-rich, soot, and Si-rich (Fruhstorfer and Niessner 1994). In our collected SEM images, we can observe that irregular dust-like structures correspond to (PM < 2.5 μm) and (PM < 10 μm) structures that are nearly spherical. EDS on those spherical particles show them to be composed mostly of carbon and oxygen with traces of Ca (see Fig. S3). It has been reported that structures with similar morphology, shape (nearly spherical) and composition (carbon, oxygen and traces of Ca) were generated from the biomass burning in the work of (Chou et al. 2008; Fruhstorfer and Niessner 1994). The deposition of compounds of many different mineral species on the surface of large dust particles is evident in our EDS analysis, refer to Fig. S3; in which, some particles related to mineral origins and some are mixed with anthropogenic origins (like biomass, burning or incomplete combustion) as mentioned by Pachauri (2013). It can be observed that the overall elemental composition of the dust particles is homogenous with only additions of chemicals on the surface. The EDS profiles enclosed in the orange (dry season) and blue (wet season) color box of Fig. S3.

In general, our microscopic analysis images showed a dominance of mineral and round shape alike fly ash components regardless of the seasonality. Two exceptions are Fig. 6b, d in which its rounded or oval shape and its chemical composition of C, O, N, Na and Ca are probably part of biological particles, similar shapes are described by Priyamvada et al. (2017). During the wet season, we noticed a predominance of larger particles (corresponding to TSP, except fig. S3-g) some shapeless and some with rounded shape and rough surfaces. From our early findings, we can

conclude that macro particles and C-rich, N-rich, Al-rich, Si-rich, Mg-rich, Ca-rich, Fe-rich and fly ash alike counted as dominant pollutants under the wet regime. This information is encompassed with the data presented in Fig. 5a–c (dry season) and 5b (wet season); in which, the pollution footprint is reduced during rainy periods.

We hypothesized that less variety and the absence of PM_{10} and $PM_{2.5}$ particles may be due the current sampling technique that may be not suitable to work under adverse meteorological conditions, with a high precipitation rate (>70 mm day^{-1})and high relative humidity ($>90\%$); in such conditions, some ambient particles may be affected by hygroscopicity (Posfai and Buseck 2010; Pöhlker et al. 2014). Our preliminary findings on this matter are not conclusive but a close approach of the airborne particles found in the environment. Further studies must be conducted to fully understand the underlying mechanisms that the role of the city's landscape, meteorology, seasonality may have on urban aerosol composition.

4 Conclusions

After 14 months of continuous monitoring of particle concentrations in the city of Guayaquil, no environmental threat was found during the evaluated period. PM_{10} and $PM_{2.5}$ mean values are within thresholds allowed by regulations from local government during 2015 and 2016.

Seasonality play an important role in the measurement of PM concentrations and their sources. We note that rains during the wet season, help to reduce the suspended particles within the city particularly during the months of February and March; while in January and May are more heterogeneous and PM increased at times during the absence of rain. Contrary, during the dry season, PM concentrations are more consistent from August to November regardless the particle size.

The south and south-west path helps to move fresh marine air masses into the city as long-range transport, which is corroborate with the meteorological data. Guayaquil city has a smooth topography, and it is protected by the gulf of Guayaquil and experiences a direct exposure of south and south-west trade winds.

Satellite data help to understand urban pollution with air masses backward trajectories, rain patterns, AOD and NO_2. The total vertical column NO_2 helps: i) to visualize the local pollution footprint of the whole city, ii) to identify possible pollution hotspots and its relationship with anthropogenic activities, and iii) to show the pollution plume of the NO_2 differs through the year, broader during the dry season and narrower during the wet season. Our findings suggest that the complexity of urban pollution, may be part of the contributor enhanced by long-range transport pollutants and drought particularly during the second half of the year.

The microscopic analysis of the ambient aerosols shows that two main groups of samples: i) large and coarse mode particles (PM_{10} and $PM_{2.5}$) with irregular shape and aggregate alike shapes, most likely corresponding to urban dust and mineral origins, and ii) other shapes like round shape and irregular shape particles with C-rich, N-rich, Al-rich, Si-rich, Mg-rich, Ca-rich and Fe-rich belonging to the coarse mode particles (PM_{10}). We note that although most of the sampled particles are uniform, some of them contain deposit or coating with materials on the surface that have additional chemical composition, which may be an indication of mixed or secondary organic aerosol particles. A comparison of SEM images of samples collected during the dry and wet seasons shows that there is a similarity in the morphological characteristics of the structures.

In summary, we considered the results presented in this study to be the first insight for further studies particularly over the interaction of a middle size south American city and its growth in the coming years. Hence, the microscopic analysis is the first step towards understanding the current state and nature of the suspended particles in the air.

Supplementary Information The online version contains supplementary material available at https://doi.org/10.1007/s41810-021-00117-2.

Acknowledgements We would like to thank Drs. Christopher Pöhlker, David Walter, Tobias Könnemann from the Max Planck Institute for Chemistry for their advice and fruitful collaborations. DMZ acknowledge the support by the German Federal Ministry of Education (BMBF contract 01LB1001A). ERC highly acknowledges the support by the GLOB-CRUST project (EMERGIA20_0033) founded by the Consejería de transformación económica industria, conocimiento y universidades de la Junta de Andalucía and the UAL-Hipatia postdoctoral fellowship funded by Plan Propio of the University of Almería. We would like to thank: Ing. Marco Valencia from LATAM airlines-Ecuador, Dr. Lok Lamsal from GESTAR-affiliated Research Scientist at NASA Goddard Space Flight Center, Mg. Fernando Ayala and Ing. Roberto Jurado from Benemérito Cuerpo de Bomberos de Guayaquil, Ing. Marco Pazmiño, Ing. Héctor Ayon, Dr. Ángel Ramírez, Msc. Mario Patiño, from ESPOL, and to Bsc. David Hernick, Dr. David Carslaw for the support to the open software community. The authors gratefully acknowledge the NOOA Air Resources Laboratory (ARL) for the provision of the HYSPLIT transport and dispersion model and/or READY website (http://www.ready.noaa.gov, last access June 2, 2021) and the Sentinel 5 Precursor TROPOMI level 2 product (http://www.tropomi.eu/data-products/nitrogen-dioxide, last access July 7, 2021) developed with funding from the Netherlands Space Office (NSO) and processed with funding from the European Space Agency (ESA) used in this publication.

Funding Open Access funding enabled and organized by Projekt DEAL.

Declarations

Conflict of interest On behalf of all authors, the corresponding author states that there is no conflict of interest.

References

Andreae MO, Acevedo OC, Araùjo A, Artaxo P, Barbosa CGG, Barbosa HMJ, Brito J, Carbone S, Chi X, Cintra BBL, da Silva NF, Dias NL, Dias-Júnior CQ, Ditas F, Ditz R, Godoi AFL, Godoi RHM, Heimann M, Hoffmann T, Kesselmeier J, Könemann T, Krüger ML, Lavric JV, Manzi AO, Lopes AP, Martins DL, Mikhailov EF, Moran-Zuloaga D, Nelson BW, Nölscher AC, Santos Nogueira D, Piedade MTF, Pöhlker C, Pöschl U, Quesada CA, Rizzo LV, Ro CU, Ruckteschler N, Sá LDA, de Oliveira Sá M, Sales CB, dos Santos RMN, Saturno J, Schöngart J, Sörgel M, de Souza CM, de Souza RAF, Su H, Targhetta N, Tóta J, Trebs I, Trumbore S, van Eijck A, Walter D, Wang Z, Weber B, Williams J, Winderlich J, Wittmann F, Wolff S, Yáñez-Serrano AM (2015) The Amazon Tall Tower Observatory (ATTO): overview of pilot measurements on ecosystem ecology, meteorology, trace gases, and aerosols. Atmos Chem Phys 15 (18):10723–10776. https://doi.org/10.5194/acp-15-10723-2015

Abdelkader M, Metzger S, Steil B, Klingmuller K, Tost H, Pozzer A, Stenchikov G, Barrie L, Lelieveld J (2017) Sensitivity of transatlantic dust transport to chemical aging and related atmospheric processes. Atmos Chem Phys 17(6):3799–3821. https://doi.org/10.5194/acp-17-3799-2017

Acker J, Soebiyanto R, Kiang R, Kempler S (2014) Use of the NASA Giovanni Data System for Geospatial Public Health Research: Example of Weather-Influenza Connection. ISPRS Int Geo-Inf 3(4):1372–1386. https://doi.org/10.3390/ijgi3041372

Andreae M (1995) Chapter 10 climatic effects of changing atmospheric aerosol levels. World Survey Climatol. https://doi.org/10.1016/S0168-6321(06)80033-7

Astudillo-Alemán M-O, García-Orellana NB, González-Arévalo GJ, Guitiérrez-Valle IA, Bailón-Bosco NC (2015) Caracterización química del material particulado PM10 de la zona urbana de Cuenca- Ecuador e investigación de su genotoxicidad e inducción de estrés oxidativo en células epiteliales alveolares A549. Rev Toxicol 31(2):121–126

Ault AP, Peters TM, Sawvel EJ, Casuccio GS, Willis RD, Norris GA, Grassian VH (2012) Single-particle SEM-EDX analysis of iron-containing coarse particulate matter in an urban environment: sources and distribution of iron within Cleveland. Ohio Environ Sci Technol 46(8):4331–4339. https://doi.org/10.1021/es204006k

Bandowe BAM, Fränkl L, Grosjean M, Tylmann W, Mosquera PV, Hampel H, Schneider T (2018) A 150-year record of polycyclic aromatic compound (PAC) deposition from high Andean Cajas National Park, southern Ecuador. Sci Total Environ 621:1652–1663. https://doi.org/10.1016/j.scitotenv.2017.10.060

Baron PA, Willeke K (2001) Aerosol measurement: principles, techniques, and applications. Wiley

Borbor M, Barriga A (2007) Integración de salud, ambiente y comunidad para evaluar la calidad del aire en zonas populares de Guayaquil y proponer acciones sociales y políticas municipales. Escuela Superior Politécnica del Litoral, Guayaquil

Bravo Alvarez H, Sosa Echeverria R, Sanchez Alvarez P, Krupa S (2012) Air quality standards for particulate matter (PM) at high altitude cities. Environ Pollut 173:255–256. https://doi.org/10.1016/j.envpol.2012.09.025

Burkhardt J (2010) Hygroscopic particles on leaves: nutrients or desiccants? Ecol Monogr 80(3):369–399. https://doi.org/10.1890/09-1988.1

Cañadas Cruz LC (1983) El mapa bioclimático y ecológico del Ecuador. Banco Central del Ecuador

Carslaw DC, Beevers SD (2013) Characterising and understanding emission sources using bivariate polar plots and k-means clustering. Environ Model Softw 40:325–329. https://doi.org/10.1016/j.envsoft.2012.09.005

Carslaw DC, Ropkins K (2012) openair — An R package for air quality data analysis. Environ Model Softw 27–28:52–61. https://doi.org/10.1016/j.envsoft.2011.09.008

Cazorla M (2016) Air quality over a populated Andean region: Insights from measurements of ozone, NO, and boundary layer depths. Atmos Pollut Res 7(1):66–74. https://doi.org/10.1016/j.apr.2015.07.006

Chou C, Formenti P, Maille M, Ausset P, Helas G, Harrison M, Osborne S (2008) Size distribution, shape, and composition of mineral dust aerosols collected during the African Monsoon Multidisciplinary Analysis Special Observation Period 0: Dust and Biomass-Burning Experiment field campaign in Niger, January 2006. J Geophys Res Atmos. https://doi.org/10.1029/2008JD009897

Delgado A (2013) Guayaquil. Cities 31:515–532. https://doi.org/10.1016/j.cities.2011.11.001

Després V, Huffman JA, Burrows SM, Hoose C, Safatov A, Buryak G, Fröhlich-Nowoisky J, Elbert W, Andreae M, Pöschl U, Jaenicke R (2012) Primary biological aerosol particles in the atmosphere: a review. Tellus b Chem Phys Meteorol 64(1):15598. https://doi.org/10.3402/tellusb.v64i0.15598

Di Biagio C, Formenti P, Balkanski Y, Caponi L, Cazaunau M, Pangui E, Journet E, Nowak S, Caquineau S, Andreae MO, Kandler K, Saeed T, Piketh S, Seibert D, Williams E, Doussin JF (2017) Global scale variability of the mineral dust long-wave refractive index: a new dataset of in situ measurements for climate modeling and remote sensing. Atmos Chem Phys 17(3):1901–1929. https://doi.org/10.5194/acp-17-1901-2017

Draxler R, Barbara S, Rolph G, Ariel S, Albion T (2018) HYSPLIT4 user's guide. National Oceanic and Atmospheric Administration

EDAX (2006) Genesis Spectrum user manual. EDAX

Eficacitas (2007) Plan de Gestión de la calidad del aire en la ciudad de Guayaquil, Volumen II Plan para el Quinquenio 2007–2012. Abril, Guayaquil Ecuador

FLACSO, MAE, PNUMA (2008) GEO Ecuador 2008: Informe sobre el estado del Medio Ambiente. Ministerio de Agricultura del Ecuador, Quito Ecuador

Fröhlich-Nowoisky J, Burrows SM, Xie Z, Engling G, Solomon PA, Fraser MP, Mayol-Bracero OL, Artaxo P, Begerow D, Conrad R, Andreae MO, Després VR, Pöschl U (2012) Biogeography in the air: fungal diversity over land and oceans. Biogeosciences 9(3):1125–1136. https://doi.org/10.5194/bg-9-1125-2012

Fruhstorfer P, Niessner R (1994) Identification and classification of airborne soot particles using an automated SEM/EDX. Microchim Acta 113(3):239–250. https://doi.org/10.1007/BF01243614

Gago EJ, Roldan J, Pacheco-Torres R, Ordóñez J (2013) The city and urban heat islands: a review of strategies to mitigate adverse effects. Renew Sustain Energy Rev 25:749–758. https://doi.org/10.1016/j.rser.2013.05.057

García-Franco JL (2020) Air quality in Mexico city during the fuel shortage of January 2019. Atmos Environ 222:117131. https://doi.org/10.1016/j.atmosenv.2019.117131

García-Garizábal I (2017) Rainfall variability and trend analysis in coastal arid Ecuador. Int J Climatol 37(13):4620–4630. https://doi.org/10.1002/joc.5110

Genga A, Siciliano T, Siciliano M, Aiello D, Tortorella C (2018) Individual particle SEM-EDS analysis of atmospheric aerosols in rural, urban, and industrial sites of Central Italy. Environ Monit Assess 190(8):456. https://doi.org/10.1007/s10661-018-6826-9

Gramsch E, Morales L, Baeza M, Ayala C, Soto C, Neira J, Pérez P, Moreno F (2020) Citizens' surveillance micro-network for the mapping of PM2.5 in the City of Concón, Chile. Aerosol Air Qual Res 20(2):358–368. https://doi.org/10.4209/aaqr.2019.04.0179

Grange SK, Lewis AC, Carslaw DC (2016) Source apportionment advances using polar plots of bivariate correlation and regression statistics. Atmos Environ 145:128–134. https://doi.org/10.1016/j.atmosenv.2016.09.016

Hand JL, Schichtel BA, Pitchford M, Malm WC, Frank NH (2012) Seasonal composition of remote and urban fine particulate matter in the United States. J Geophys Res Atmos. https://doi.org/10.1029/2011JD017122

Holecek JC, Spencer MT, Prather KA (2007) Analysis of rainwater samples: comparison of single particle residues with ambient particle chemistry from the northeast Pacific and Indian oceans. J Geophys Res Atmos. https://doi.org/10.1029/2006JD008269

Johansson E, Yahia MW, Arroyo I, Bengs C (2018) Outdoor thermal comfort in public space in warm-humid Guayaquil, Ecuador. Int J Biometeorol 62(3):387–399. https://doi.org/10.1007/s00484-017-1329-x

Juneng L, Latif MT, Tangang FT, Mansor H (2009) Spatio-temporal characteristics of PM10 concentration across Malaysia. Atmos Environ 43(30):4584–4594. https://doi.org/10.1016/j.atmosenv.2009.06.018

Kahn RA, Limbacher J (2012) Eyjafjallajokull volcano plume particle-type characterization from space-based multi-angle imaging. Atmos Chem Phys 12(20):9459–9477. https://doi.org/10.5194/acp-12-9459-2012

Krotkov NA, Lamsal LN, Celarier EA, Swartz WH, Marchenko SV, Bucsela EJ, Chan KL, Wenig M, Zara M (2017) The version 3 OMI NO2 standard product. Atmos Meas Tech 10(9):3133–3149. https://doi.org/10.5194/amt-10-3133-2017

Lelieveld J, Evans JS, Fnais M, Giannadaki D, Pozzer A (2015) The contribution of outdoor air pollution sources to premature mortality on a global scale. Nature 525(7569):367–371. https://doi.org/10.1038/nature15371

Li W, Shao L, Shen R, Yang S, Wang Z, Tang U (2011) Internally Mixed Sea Salt, Soot, and Sulfates at Macao, a Coastal City in South China. J Air Waste Manag Assoc 61:1166–1173. https://doi.org/10.1080/10473289.2011.603996

Luna MAG, Luna FAG, Espinosa JFM, Ceron LCB (2018) Spatial and temporal assessment of particulate matter using AOD data from MODIS and surface measurements in the ambient air of Colombia. Asian J Atmos Environ 12(2):165–177. https://doi.org/10.5572/ajae.2018.12.2.165

MAE (2011) Norma Ecuatoriana de calidad del aire. Ministerio de Ambiente, Quito

Martins LD, Wikuats CFH, Capucim MN, de Almeida DS, da Costa SC, Albuquerque T, Barreto Carvalho VS, de Freitas ED, de Fátima AM, Martins JA (2017) Extreme value analysis of air pollution data and their comparison between two large urban regions of South America. Weather Clim Extremes 18:44–54. https://doi.org/10.1016/j.wace.2017.10.004

Miao Y, Li J, Miao S, Che H, Wang Y, Zhang X, Zhu R, Liu S (2019) Interaction between planetary boundary layer and PM2.5 pollution in megacities in China: a review. Curr Pollut Reports 5(4):261–271. https://doi.org/10.1007/s40726-019-00124-5

Moffet RC (2011) Scanning transmission X-ray microscopy: applications in atmospheric aerosol research. http://escholarship.org/uc/item/0gh7r6z4

Morillas H, Maguregui M, García-Florentino C, Marcaida I, Madariaga JM (2016) Study of particulate matter from Primary/Secondary Marine Aerosol and anthropogenic sources collected by a self-made passive sampler for the evaluation of the dry deposition impact on built heritage. Sci Total Environ 550:285–296. https://doi.org/10.1016/j.scitotenv.2016.01.080

Nousiainen T (2009) Optical modeling of mineral dust particles: a review. J Quant Spectrosc Radiat Transfer 110(14):1261–1279. https://doi.org/10.1016/j.jqsrt.2009.03.002

Pachauri T (2013) SEM-EDX characterization of individual coarse particles in Agra, India. Aerosol and Air Quality Research. https://doi.org/10.4209/aaqr.2012.04.0095

Parra R (2018) Performance studies of planetary boundary layer schemes in WRF-Chem for the Andean region of Southern Ecuador. Atmos Pollut Res 9(3):411–428. https://doi.org/10.1016/j.apr.2017.11.011

Perrone MR, Romano S, Genga A, Paladini F (2018) Integration of optical and chemical parameters to improve the particulate matter characterization. Atmos Res 205:93–106. https://doi.org/10.1016/j.atmosres.2018.02.015

Pinto EB, Slowey NC (2021) Stable isotope evidence for the origins of waters in the Guayas estuary and Gulf of Guayaquil. Estuar Coast Shelf Sci 250:107151. https://doi.org/10.1016/j.ecss.2020.107151

Pöhlker C, Saturno J, Krüger ML, Förster J-D, Weigand M, Wiedemann KT, Bechtel M, Artaxo P, Andreae MO (2014) Efflorescence upon humidification? X-ray microspectroscopic in situ observation of changes in aerosol microstructure and phase state upon hydration. Geophysi Res Lett 41(10):2014GL059409. https://doi.org/10.1002/2014GL059409

Pöhlker C, Walter D, Paulsen H, Könemann T, Rodríguez-Caballero E, Moran-Zuloaga D, Brito J, Carbone S, Degrendele C, Després VR, Ditas F, Holanda BA, Kaiser JW, Lammel G, Lavrič JV, Ming J, Pickersgill D, Pöhlker ML, Praß M, Löbs N, Saturno J, Sörgel M, Wang Q, Weber B, Wolff S, Artaxo P, Pöschl U, Andreae MO (2019) Land cover and its transformation in the backward trajectory footprint region of the Amazon Tall Tower Observatory. Atmos Chem Phys 19(13):8425–8470. https://doi.org/10.5194/acp-19-8425-2019

Pöschl U (2005) Atmospheric aerosols: composition, transformation, climate and health effects. Angew Chem Int Ed 44(46):7520–7540. https://doi.org/10.1002/anie.200501122

Posfai M, Buseck PR (2010) Nature and climate effects of individual tropospheric aerosol particles. In: Jeanloz R, Freeman KH (eds) annual review of earth and planetary sciences, Vol 38, vol 38. Annual review of earth and planetary sciences. Annual reviews, Palo Alto, pp 17–43. https://doi.org/10.1146/annurev.earth.031208.100032

Priyamvada H, Akila M, Singh RK, Ravikrishna R, Verma RS, Philip L, Marathe RR, Sahu LK, Sudheer KP, Gunthe SS (2017) Terrestrial macrofungal diversity from the tropical dry evergreen biome of Southern India and its potential role in aerobiology. PLoS ONE 12(1):e0169333. https://doi.org/10.1371/journal.pone.0169333

Rissler J, Nordin EZ, Eriksson AC, Nilsson PT, Frosch M, Sporre MK, Wierzbicka A, Svenningsson B, Löndahl J, Messing ME, Sjogren S, Hemmingsen JG, Loft S, Pagels JH, Swietlicki E (2014) Effective density and mixing state of aerosol particles in a near-traffic urban environment. Environ Sci Technol 48(11):6300–6308. https://doi.org/10.1021/es5000353

Samek L, Stegowski Z, Styszko K, Furman L, Fiedor J (2018) Seasonal contribution of assessed sources to submicron and fine particulate

matter in a Central European urban area. Environ Pollut 241:406–411. https://doi.org/10.1016/j.envpol.2018.05.082

Seinfeld JH, Pandis SN (1998) Atmospheric chemistry and physics. Wiley, New York

Silva J, Rojas J, Norabuena M, Molina C, Toro RA, Leiva-Guzman MA (2017) Particulate matter levels in a South American megacity: the metropolitan area of Lima-Callao. Peru Environ Monit Assess. https://doi.org/10.1007/s10661-017-6327-2

Soto-Coloballes N (2020) The development of air pollution in Mexico City. SAGE Open 10(2):2158244020931072. https://doi.org/10.1177/2158244020931072

Stein AF, Draxler RR, Rolph GD, Stunder BJB, Cohen MD, Ngan F (2015) NOAA's HYSPLIT atmospheric transport and dispersion modeling system. Bull Am Meteorol Soc 96(12):2059–2077. https://doi.org/10.1175/BAMS-D-14-00110.1

Steinle S, Reis S, Sabel CE, Semple S, Twigg MM, Braban CF, Leeson SR, Heal MR, Harrison D, Lin C, Wu H (2015) Personal exposure monitoring of PM2.5 in indoor and outdoor microenvironments. Sci Total Environ 508:383–394. https://doi.org/10.1016/j.scitotenv.2014.12.003

Thiel M, Macaya E, Acuna E, Arntz W, Bastias H, Brokordt K, Camus P, Castilla J, Castro L, Cortes M, Dumont C, Escribano R, Fernandez M, Gajardo J, Gaymer C, Gomez I, Gonzalez A, González HE, Haye P, Vega JMA (2007) The Humboldt current system of Northern and Central Chile. Oceanogr Mar Biol 45:195–345. https://doi.org/10.1201/9781420050943.ch6

Vargas FA, Rojas NY, Pachon JE, Russell AG (2012) PM10 characterization and source apportionment at two residential areas in Bogota. Atmos Pollut Res 3(1):72–80. https://doi.org/10.5094/APR.2012.006

Vercellino RJ, Sleeth DK, Handy RG, Min KT, Collingwood SC (2018) Laboratory evaluation of a low-cost, real-time, aerosol multi-sensor. J Occup Environ Hyg 15(7):559–567. https://doi.org/10.1080/15459624.2018.1468565

Wang J, Ogawa S (2015) Effects of meteorological conditions on PM2.5 concentrations in Nagasaki, Japan. Int J Environ Res Public Health 12(8):9089

Zalakeviciute R, López-Villada J, Rybarczyk Y (2018a) Contrasted effects of relative humidity and precipitation on urban PM2.5 pollution in high elevation urban areas. Sustainability 10(6):2064

Zalakeviciute R, Rybarczyk Y, López-Villada J, Diaz Suarez MV (2018b) Quantifying decade-long effects of fuel and traffic regulations on urban ambient PM2.5 pollution in a mid-size South American city. Atmos Pollut Res 9(1):66–75. https://doi.org/10.1016/j.apr.2017.07.001

Zalakeviciute R, Rybarczyk Y, Granda-Albuja MG, Diaz Suarez MV, Alexandrino K (2020) Chemical characterization of urban PM10 in the Tropical Andes. Atmos Pollut Res 11(2):343–356. https://doi.org/10.1016/j.apr.2019.11.007

Zhang D, Liu J, Li B (2014) Tackling air pollution in China—what do we learn from the great smog of 1950s in LONDON. Sustainability 6(8):5322

Zhao X, Griffin D, Fioletov V, McLinden C, Cede A, Tiefengraber M, Müller M, Bognar K, Strong K, Boersma F, Eskes H, Davies J, Ogyu A, Lee SC (2020) Assessment of the quality of TROPOMI high-spatial-resolution NO2 data products in the Greater Toronto Area. Atmos Meas Tech 13(4):2131–2159. https://doi.org/10.5194/amt-13-2131-2020

Zhou Y, Yue Y, Bai Y, Zhang L (2020) Effects of rainfall on PM2.5 and PM10 in the Middle Reaches of the Yangtze River. Adv Meteorol. https://doi.org/10.1155/2020/2398146